Forced desorption of nanoparticles from an oil-water interface

Valeria Garbin, John C. Crocker, Kathleen J. Stebe[*]

Department of Chemical and Biomolecular Engineering, University of Pennsylvania,

220 S. 33rd St., Philadelphia, Pennsylvania, 19104-6393, USA.

ABSTRACT While nanoparticle adsorption to fluid interfaces has been studied from a fundamental standpoint and exploited in application, the reverse process, i.e. desorption and disassembly, remains relatively unexplored. Here we demonstrate the forced desorption of gold nanoparticles capped with amphiphilic ligands from an oil-water interface. A monolayer of nanoparticles is allowed to spontaneously form by adsorption from an aqueous suspension onto a drop of oil, and is subsequently compressed by decreasing the drop volume. The surface pressure is monitored by pendant drop tensiometry throughout the process. Upon compression, the nanoparticles are mechanically forced out of the interface into the aqueous phase. An optical method is developed to measure the nanoparticle area density *in situ*. We show that desorption occurs at a coverage that corresponds to close packing of the ligand-capped particles, suggesting that ligand-induced repulsion plays a crucial role in this process.

[*] kstebe@seas.upenn.edu

Introduction

The spontaneous assembly of nanoparticles to form *adsorbed monolayers* at fluid-fluid interfaces has been exploited for stabilization of emulsions and foams[1-5], for creating capsules and nanoporous membranes[6-8], and has found application in phase-transfer catalysis[9,10] and enhanced oil recovery[11]. The outcome of such processes and applications relies on the mechanical and kinetic properties of the nanoparticle monolayer in dynamic settings; therefore, understanding their dynamic response is of great interest. While recent studies have addressed the kinetics of nanoparticle adsorption to quiescent interfaces[12,13], little is known about the response of the resulting monolayers to deformation.

There has been significant research on the mechanical response of particle-laden fluid interfaces using *spread monolayers* as model systems. Experiments have revealed a solid-like behavior[14-22] and in some instances, particle expulsion into one of the fluid phases[23-25]. This range of behavior is reminiscent of that of spread monolayers of lipids under strong compression: condensed monolayers exhibit solid-like response and collapse by folding, while monolayers that remain liquid expel material in the fluid subphase[26]. Spread monolayers are prepared by depositing particles on a fluid subphase by a spreading solvent, which may introduce effects not present in systems where the particles adsorb spontaneously. Therefore, it is of interest to study directly the dynamic response of adsorbed nanoparticle monolayers. Since the interface is an "open system" that can exchange nanoparticles with the surrounding suspension, this is a particularly challenging task. To date, only a few studies have addressed this problem, and a solid-like behavior[27, 28] has been observed, including buckling of the monolayer under strong compression[29, 30].

In this Letter we demonstrate the mechanically forced desorption of nanoparticles adsorbed at an oil-water interface. We study an interfacial monolayer of nanoparticles formed by adsorption onto a pendant drop. By expanding and contracting the drop, we can manipulate the area density of nanoparticles while simultaneously measuring the surface tension of the composite interface. To understand the conditions in which the nanoparticles desorb, we developed an optical method to quantify their area density. Desorption was observed at an area density that corresponds to close

packing of ligand-capped nanoparticles. The measured desorption energy of a particle confirms the important role of ligands in the process.

The results presented here demonstrate that controlled interfacial assembly and disassembly of nanoparticles from suspension can be achieved. This mechanism should facilitate the recovery and recycling of potentially expensive components, thereby improving the sustainability of processes in which nanoparticles are exploited[31,32].

Results and Discussion

Gold nanoparticles stabilized by the amphiphilic ligand thioalkylated tetraethylene glycol[33] spontaneously adsorb at water-trichlorobenzene[8] and water-octafluoropentylacrylate[13] (OFPA) interfaces. For this study we used the latter system, with gold (Au) cores of radii $a_{core} = 2.3\,\text{nm}$ and $a_{core} = 5\,\text{nm}$, respectively. The capping ligand, (1-mercaptoundec-11-yl)tetra(ethylene glycol) (MUTEG), is uncharged and provides stability to the colloidal suspension by short-range steric repulsion; once grafted, the hydrophobic block of the ligand is adjacent to the particle. Interactions between neighboring particles depend on the configuration of both the hydrophobic block (undecane, contour length ~ 1 nm) and the hydrophilic block (tetraethylene glycol, contour length ~ 1.5 nm). Recent molecular dynamics simulations[34] of nanoparticles with amphiphilic capping ligands similar to MUTEG suggest that the degree of extension of the hydrophilic and hydrophobic blocks depends not only on the solvent conditions, but also on the grafting density of ligands. For instance, in water, the hydrophobic blocks can remain extended provided that the brush is sufficiently dense that water cannot penetrate the layer. The grafting density of the ligand on the particles used in the experiments is not known precisely.

We formed a pendant drop of OFPA from the tip of a needle in an aqueous suspension of Au-MUTEG nanoparticles ($a_{core} = 2.3\,\text{nm}$; bulk concentration: $n = 1.9 \times 10^{14}\,\text{NPs/mL}$; volume fraction: $\phi \approx 10^{-5}$). Figure 1(a-b) shows that, as the nanoparticles spontaneously adsorb at the fluid-fluid interface, the surface layer of particles attenuates the transmitted light and the drop becomes darker. This effect can be quantified by measuring the optical absorbance $\mathcal{A} = -\ln\left(I/I_0\right)$ where I and

I_0 are the intensities of the light transmitted at the center of the drop and outside the drop, respectively. Since $\mathcal{A}$ is a monotonically increasing function of the area density of particles $\Gamma = N_s / A$ (see S.I.), the darker the drop, the higher the area density. Upon compression, the increase in Γ is confirmed by a further increase in the absorbance (Figure 1(c)). At high area density the particles desorb (Figure 1(d)) and form a diffuse cloud surrounding the drop. Following desorption, the cloud of particles sediments (Figure 1(e-f)) exhibiting the well-known behavior of a dense suspension immersed in a fluid of lower mass density[35,36] known as streaming (see the Supporting Information).
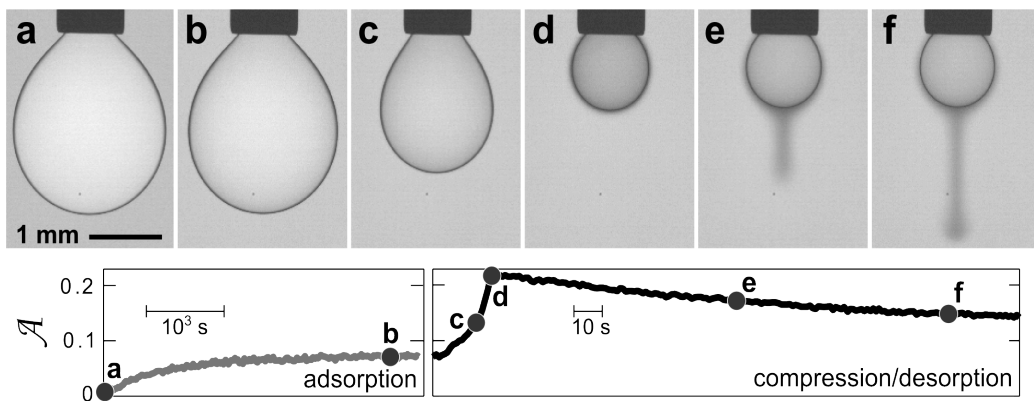

Figure 1. Desorption of Au-MUTEG nanoparticles ($a_{core} = 2.3\,\mathrm{nm}$) from a compressed oil-water interface. The plots show the time evolution of the optical absorbance $\mathcal{A}$ during the various stages of the process. (a) A clean drop of OFPA is initially formed in a suspension of nanoparticles ($\mathcal{A} = 0$). (b) Nanoparticles spontaneously adsorb at the oil-water interface ($\mathcal{A}$ increases). (c) The drop is compressed, leading to a higher area density of particles ($\mathcal{A}$ further increases). (d) Nanoparticles desorb from the interface, forming a cloud around the drop. (e-f) The cloud of particles sediments ($\mathcal{A}$ decreases).

Drop shape analysis enables us to extract the effective surface tension of the composite interface at all stages of the process[37]. The adsorbed particles generate a two-dimensional surface pressure[2,12,13,38,39] Π, owing to configurational entropy and ligand-mediated interparticle repulsion, which varies with drop compression. As a result, the measured surface tension $\gamma = \gamma_0 - \Pi$ is smaller than that of the bare interface γ_0.

4

As the adsorption of Au-MUTEG nanoparticles onto the OFPA-water interface proceeds, the surface tension $\gamma(t)$ progressively decreases. The time for the surface tension to reach its equilibrium value for a suspension of similar volume fraction has been previously determined[13] to be ~10^5 s, and the minimum value of the surface tension ≈ 13 mN/m. Here, we let adsorption proceed only until the rate of change $d\gamma/dt$ is sufficiently small that the number of particles on the interface N_s can be considered constant over the time scale of the subsequent compression experiment (~100 s), enabling us to measure the area density $\Gamma = N_s/A$ during compression from a single measurement of N_s. Figure 2(a) shows that after 4000 s the rate of change of the surface tension is $d\gamma/dt \approx -10^{-4}$ mN m^{-1}s^{-1}. We typically incubate the drops for ~10^3 s prior to compression, with a resulting initial surface pressure $\Pi \approx 1.5$–2 mN m^{-1}. A small fraction of the decrease in surface tension is ascribed to the presence of traces of MUTEG ligands in solution that co-adsorb at the OFPA-water interface, but control experiments verify that the co-adsorbed molecules do not significantly influence the phenomena reported here (see S.I.).

A typical compression experiment is reported in Figure 2(b). From an initial surface pressure $\Pi \approx 2$ mN m^{-1}, the drop is compressed by withdrawing liquid, at a constant rate of change of the area $dA/dt \approx -0.1$ mm^{2}s^{-1}. As the drop is compressed, the surface pressure increases until a plateau is reached. The plateau corresponds to desorption of the nanoparticles[23]; the critical pressure Π_c is identified as the point where the slope of the $\Pi(A)$ curve begins to decrease.

Desorption reproducibly occurs at $\Pi_c \approx 13$ mN m^{-1}. This value is consistent with the minimum surface tension reported in Ref. 13. A collapse pressure $\Pi_c << \gamma_0$ is the signature of a monolayer that remains fluid and hence can desorb. This is in marked contrast to the phenomenon of buckling, observed for solid-like monolayers[15,18,30]. When the monolayer behaves like a solid, Π can approach the value of the surface tension of the bare interface γ_0, i.e. the effective surface tension $\gamma = \gamma_0 - \Pi$ can go to zero[15,28] and the composite interface behaves as a tensionless film.
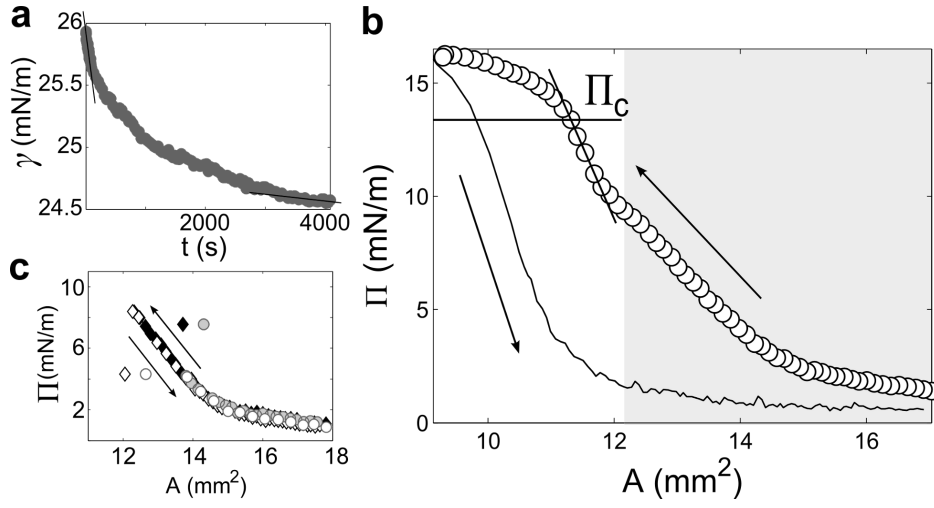
Figure 2. (a) Dynamic surface tension of the OFPA-water interface ($\gamma_0 = 26$ mN/m) during adsorption of Au-MUTEG nanoparticles with $a_{core} = 2.3$ nm. (b) Surface pressure $\Pi = \gamma_0 - \gamma$ upon compression. The plateau at the collapse pressure Π_c is indicative of desorption. The shaded area in (b) is reversible upon compression/expansion cycles, as shown in (c).

Because particles have desorbed, the $\Pi(A)$ curve in Figure 2(b) is not reversible, as seen upon re-expansion of the drop (solid line). To check for reversibility, we run cycles of compression/expansion below Π_c; the $\Pi(A)$ curve is indeed reversible and independent of compression rate for cycles of amplitude sufficiently small that $\Pi < 10\,\text{mN}\,\text{m}^{-1}$, as shown in Figure 2(c). However, if the compression is arrested in the range $10 < \Pi < 13\,\text{mN}\,\text{m}^{-1}$ and the drop is subsequently re-expanded, weak hysteresis is observed, although desorption does not yet occur. This may be related to the presence of trace ligands co-adsorbed at the OFPA-water interface. We make use of the reversibility of the $\Pi(A)$ curve in the range $\Pi < 10\,\text{mN}\,\text{m}^{-1}$ in the measurement of N_s as described below.

The work done upon compression to induce the desorption of one particle can be estimated as $W = \Pi_c\,dA$, where dA is the change in area of the interface upon expulsion of the particle. To measure this quantity directly, we developed a method to quantify the area density of particles Γ. The compression experiments are intentionally performed under conditions where the number of

particles N_s is fixed (up to desorption). Thus, if N_s is known at one point of the $\Pi(A)$ curve, $\Gamma = N_s/A$ can be extracted at all other points. To determine N_s, we measure the number of particles that have desorbed from the drop (the plume visible in Figure 1(e-f)) by quantitative photometry. We compare $\Pi(A)$ curves of the drop before and after desorption; the area scaling that collapses the curves onto each other is the ratio of the number of interfacial particles before and after desorption. This scaling can be performed reliably in the range of surface pressure where the $\Pi(A)$ curves are reversible (see Figure 2(c)). Details on the method can be found in the Supporting Information. To our knowledge, this is the first *in situ* determination of the area density of nanoparticles adsorbed at fluid-fluid interfaces.
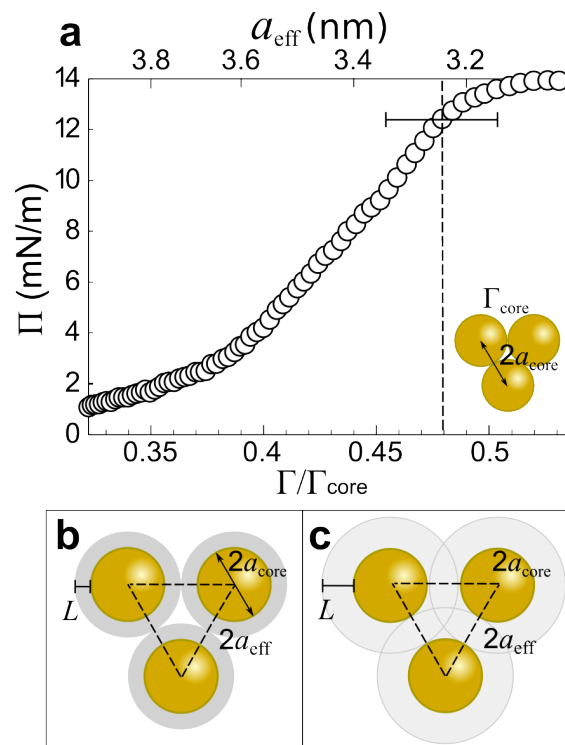

Figure 3. Desorption is observed at Γ significantly below the maximum area density Γ_{core} of the Au cores alone. (a) Surface pressure Π as a function of area density Γ (bottom axis) and effective radius a_{eff} of the nanoparticles (top axis). The area density is normalized by the value Γ_{core} corresponding to close packing of the Au cores (inset). (b) The effective radius is $a_{eff} = a_{core} + L$ if ligands form dense brushes (dark gray) that do not interpenetrate. (c) The effective radius is $a_{eff} = a_{core} + L/2$ if ligands form sparse brushes (light gray) that can interpenetrate.

Figure 3(a) shows the resulting $\Pi(\Gamma)$ curve. The area density Γ is normalized to the reference value $\Gamma_{\text{core}} \approx 5.7 \times 10^{16}$ NP m^{-2}, which is the maximum area density for the Au cores ($a_{\text{core}} = 2.3$ nm) assuming that they can attain hexagonal close packing (see inset in Figure 3(a)). Desorption is observed at Γ significantly below this packing, at an area density that corresponds to hexagonally close-packed spheres of radius $a_{\text{eff}} \approx 3.3$ nm (Figure 3(b)). This effective radius could be compatible with two scenarios. In one scenario, the ligands are grafted onto the particles' surface at high density and provide repulsion upon contact between the brushes, much like impenetrable spheres of radius $a_{\text{eff}} = a_{\text{core}} + L$ (see Figure 3(b)); the ligand length that is compatible with this scenario is $L \approx 1$ nm. The other possibility is that the grafting density of ligands is sufficiently low that the brushes can interdigitate. In this case, the contact of the brush with the Au core of another particle would give repulsion; in this scenario $a_{\text{eff}} = a_{\text{core}} + L/2$ with $L \approx 2$ nm (see Figure 3(c)). Both values of L are compatible with the known contour length of the ligand.

The work done upon compression to expel one particle is $W = \Pi_c dA \approx \Pi_c \pi a_{\text{eff}}^2 = 111\, k_{\text{B}}T$. This value can be compared to the value reported previously[13], 60 $k_{\text{B}}T$, obtained under the assumption that $\Gamma = \Gamma_{\text{core}}$. Recent molecular dynamics studies[34,40] suggest that ligand rearrangement contributes significantly to the energetics of nanoparticles at interfaces. In particular, these simulations confirm that ligands can arrange themselves into a configuration that removes fluid-fluid contact to a larger extent than would be expected from the size of the Au core alone[34]. These ligand configurations effectively prevent particle aggregation and formation of a solid-like film that could undergo buckling.

Finally, we studied the response to compression of adsorbed monolayers of larger Au-MUTEG nanoparticles, with radius $a_{\text{core}} = 5$ nm. These nanoparticles also desorb upon compression and, in addition, the monolayers show rich dynamic responses. Figure 4 shows three examples of observed behavior. In (a), desorption followed by sedimentation is visible. In (b), the interfacial layer undergoes micro-phase separation, presumably due to the presence of co-adsorbed trace ligands. Upon drop compression, the particle-rich domains collapse, forming two separate plumes of

desorbed particles. In (c), the adsorbed particles sediment on the drop surface and the particle-rich "cap" seems to be wiped off by the edge of the needle, forming a rim of desorbed particles around the drop. These data suggest that the location of desorption plumes on heterogeneous monolayers corresponds to areas of relatively dense particle packing.
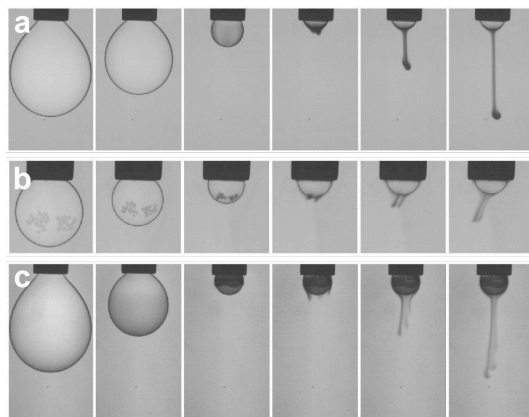

Figure 4. Desorption of Au-MUTEG nanoparticles with a_{core} = 5 nm from a compressed OFPA-water interface. In (a), a single plume of particles desorbs. In (b) microphase separation is observed; two nanoparticle plumes are expelled. In (c) sedimentation of aggregates on the interface is apparent; nanoparticles form a rim near the needle prior to desorption. (Scale: in all images, the width of the needle is 0.902 mm.)

Conclusions

In this work, we demonstrated the mechanically forced desorption of an adsorbed monolayer of ligand-capped nanoparticles from an oil-water interface. We developed an experimental method that allowed us to quantify the critical packing at which desorption occurs. The data suggest that ligand brushes on the nanoparticles play a crucial role in this process. This phenomenon may be harnessed to recover functional nanoparticles from fluid-fluid interfaces, thereby improving the economic viability or environmental sustainability of processes that exploit them.

Materials and Methods

Materials 4.5 nm (11-Mercaptoundecyl)tetra(ethylene glycol) functionalized gold nanoparticles

(Au-MUTEG) were obtained from Sigma-Aldrich (687863). 10 nm Au-MUTEG nanoparticles were acquired from NanoPartz (22-10-MUTEG). 2,2,3,3,4,4,5,5-Octafluoropentyl acrylate was obtained from Sigma-Aldrich (474401) and used as received (97%, 100 ppm monomethyl ether hydroquinone as inhibitor). The inhibitor is not surface active at the OFPA-water interface[13].

Dynamic surface tension measurements We used a pendant drop apparatus (Attension Theta) and software for fitting the drop shapes to the Young-Laplace equation. The suspension of nanoparticles was placed in a quartz cuvette (Fisher 14-385-910B). Glassware and syringe parts were carefully cleaned following standard protocols. The temperature in the laboratory was 24°C.

Supporting Information. Control experiments showing the presence of co-adsorbed trace ligands. Calibration of the specific absorbance ε of the Au-MUTEG nanoparticles ($a_{core} = 2.3\,\mathrm{nm}$). Measurement of the area density of nanoparticles Γ from a desorption experiment. Quantitative photometry of a desorption experiment. In situ photometry of the particle-laden drop and calibration of the absorbance $\mathcal{A}$ versus area density. Experiment showing streaming of a droplet of aqueous nanoparticle suspension in pure water. This material is available free of charge via the Internet at http://pubs.acs.org.

References

1. Levine, S.; Bowen, B.; Partridge, S., *Colloids and surfaces* **1989,** *38* (2), 325-343.
2. Levine, S.; Bowen, B.; Partridge, S., *Colloids and surfaces* **1989,** *38* (2), 345-364.
3. Aveyard, R.; Binks, B. P.; Clint, J. H., *Advances in Colloid and Interface Science* **2003,** *100*, 503-546.
4. Binks, B. P.; Horozov, T. S., *Angew. Chem.-Int. Edit.* **2005,** *44* (24), 3722-3725.
5. Martinez, A. C.; Rio, E.; Delon, G.; Saint-Jalmes, A.; Langevin, D.; Bink, B. P., *Soft Matter* **2008,** *4* (7), 1531-1535.
6. Lin, Y.; Skaff, H.; Emrick, T.; Dinsmore, A. D.; Russell, T. P., *Science* **2003,** *299* (5604), 226-229.
7. Duan, H.; Wang, D.; Sobal, N. S.; Giersig, M.; Kurth, D. G.; Möhwald, H., *Nano Lett.* **2005,** *5* (5), 949-952.
8. Glogowski, E.; Tangirala, R.; He, J.; Russell, T.; Emrick, T., *Nano Lett* **2007,** *7* (2), 389-393.
9. Faria, J.; Ruiz, M. P.; Resasco, D. E., *Adv. Synth. Catal.* **2010,** *352* (14-15), 2359-2364.
10. Crossley, S.; Faria, J.; Shen, M.; Resasco, D. E., *Science* **2010,** *327* (5961), 68-72.
11. Zhang, T.; Davidson, A.; Bryant, S. L.; Huh, C., Nanoparticle-Stabilized Emulsions for Applications in Enhanced Oil Recovery. In *SPE Improved Oil Recovery Symposium*, Society of Petroleum Engineers: Tulsa, Oklahoma, USA, 2010.
12. Kutuzov, S.; He, J.; Tangirala, R.; Emrick, T.; Russell, T.; Böker, A., *Phys. Chem. Chem. Phys* **2007,**

9   (48), 6351-6358.

13.   Du, K.; Glogowski, E.; Emrick, T.; Russell, T.; Dinsmore, A., *Langmuir* **2010**, 2374.

14.   Aveyard, R.; Clint, J.; Nees, D.; Paunov, V., *Langmuir* **2000,** *16* (4), 1969-1979.

15.   Aveyard, R.; Clint, J. H.; Nees, D.; Quirke, N., *Langmuir* **2000,** *16* (23), 8820-8828.

16.   Cicuta, P.; Stancik, E.; Fuller, G., *Phys. Rev. Lett.* **2003,** *90* (23), 236101.

17.   Xu, H.; Melle, S.; Golemanov, K.; Fuller, G., *Langmuir* **2005,** *21* (22), 10016-10020.

18.   Monteux, C.; Kirkwood, J.; Xu, H.; Jung, E.; Fuller, G., *Phys. Chem. Chem. Phys* **2007,** *9* (48), 6344-6350.

19.   Kubowicz, S.; Hartmann, M.; Daillant, J.; Sanyal, M.; Agrawal, V.; Blot, C.; Konovalov, O.; Mŏhwald,   H., *Langmuir* **2008,** *25* (2), 952-958.

20.   Zang, D. Y.; Rio, E.; Langevin, D.; Wei, B.; Binks, B. P., *The European Physical Journal E* **2010,** *31* (2), 125-134.

21.   Zang, D. Y.; Langevin, D.; Binks, B. P.; Wei, B., *Physical Review E* **2010,** *81*, 011604.

22.   Leahy, B.; Pocivavsek, L.; Meron, M.; Lam, K. L.; Salas, D.; Viccaro, P. J.; Lee, K. Y. C.; Lin, B., *Phys. Rev. Lett.* **2010,** *105*, 058301.

23.   Clint, J.; Taylor, S., *Colloids and surfaces* **1992,** *65* (1), 61-67.

24.   Horvolgyi, Z.; Nemeth, S.; Fendler, J. H., *Langmuir* **1996,** *12* (4), 997-1004.

25.   Bordacs, S.; Agod, A.; Horvolgyi, Z., *Langmuir* **2006,** *22* (16), 6944-6950.

26.   Gopal, A.; Lee, K. Y. C., *J. Phys. Chem. B* **2006,** *110* (44), 22079-22087.

27.   Arditty, S.; Schmitt, V.; Lequeux, F.; Leal-Calderon, F., *The European Physical Journal B* **2005,** *44* (3),   381-393.

28.   Cheng, H. L.; Velankar, S. S., *Langmuir* **2009,** *25* (8), 4412-4420.

29.   Asekomhe, S. O.; Chiang, R.; Masliyah, J. H.; Elliott, J. A. W., *Industrial & Engineering Chemistry Research* **2005,** *44* (5), 1241-1249.

30.   Datta, S. S.; Shum, H. C.; Weitz, D. A., *Langmuir* **2010,** *26* (24), 18612-18616.

31.   Myakonkaya, O.; Hu, Z. Y.; Nazar, M. F.; Eastoe, J., *Chemistry - A European Journal* **2010,** *16* (39), 11784-11790.

32.   Nazar, M. F.; Myakonkaya, O.; Shah, S. S.; Eastoe, J., *J. Colloid Interface Sci.* **2011,** *354* (2), 624-629.

33.   Kanaras, A. G.; Kamounah, F. S.; Schaumburg, K.; Kiely, C. J.; Brust, M., *Chem. Commun.* **2002,** (20),   2294-2295.

34.   Ranatunga, R.; Kalescky, R.; Chiu, C.; Nielsen, S., *J. Phys. Chem* **2010,** *100* (114), 12151-12157.

35.   Batchelor, G. K., *Journal of Fluid Mechanics* **1976,** *74* (01), 1-29.

36.   Metzger, B.; Nicolas, M.; Guazzelli, É., *Journal of Fluid Mechanics* **2007,** *580*, 283.

37.   The experiment presented in Figure 1 was designed to make desorption clearly visible. The drop shapes are not suitable for determination of surface tension since the drop becomes too small to be significantly   deformed by gravity. The rate of compression is also much faster than in the experiments presented in   Figure 2 and Figure 3.

38.   Borrell, M.; Leal, L., *Langmuir* **2007,** *23* (25), 12497-12502.

39.   Cheng, H.-L.; Velankar, S. S., *Colloids and Surfaces A: Physicochemical and Engineering Aspects* **2008,** *315* (1-3), 275-284.

40.   Tay, K. A.; Bresme, F., *Journal of the American Chemical Society* **2006,** *128* (43), 14166-14175.